

Flood–ebb and spring–neap variations of mixing, stratification and circulation in Chesapeake Bay

Ming Li*, Liejun Zhong

Horn Point Laboratory, University of Maryland Center for Environmental Science, P.O. Box 775, Cambridge, MD 21613, USA

Received 15 January 2007; received in revised form 14 May 2007; accepted 20 June 2007

Available online 5 July 2007

Abstract

A three-dimensional hydrodynamic model is used to investigate intra-tidal and spring–neap variations of turbulent mixing, stratification and residual circulation in the Chesapeake Bay estuary. Vertical profiles of salinity, velocity and eddy diffusivity show a marked asymmetry between the flood and ebb tides. Tidal mixing in the bottom boundary layer is stronger and penetrates higher on flood than on ebb. This flood–ebb asymmetry results in a north–south asymmetry in turbulent mixing because tidal currents vary out of phase between the lower and upper regions of Chesapeake Bay. The asymmetric tidal mixing causes significant variation of salinity distribution over the flood–ebb tidal cycle but insignificant changes in the residual circulation. Due to the modulation of tidal currents over the spring–neap cycle, turbulent mixing and vertical stratification show large fortnightly and monthly fluctuations. The stratification is not a linear function of the tidal-current amplitude. Strong stratification is only established during those neap tides when low turbulence intensity persists for several days. Residual circulation also shows large variations over the spring–neap cycle. The tidally averaged residual currents are about 50% stronger during the neap tides than during the spring tides.

© 2007 Elsevier Ltd. All rights reserved.

Keywords: Tidal mixing; Stratification; Estuarine circulation

1. Introduction

Recent observations in estuaries and shelf seas have revealed significant asymmetry in turbulent mixing and stratification over a tidal cycle. Jay and Smith (1990) analysed data collected from the Columbia River estuary and found a flood–ebb asymmetry: enhanced shear and stratification during ebb tides but stronger mixing and weaker stratification during flood tides. Geyer et al. (2000) estimated eddy viscosity in the Hudson River and found that flood values exceeded ebb values by a factor of 2. Other estuarine field studies have also documented this tidal asymmetry and suggested that the asymmetric mixing needs to be considered when calculating tidally averaged vertical fluxes (Stacey et al. 2001; Peters and Bokhorst, 2001). Stacey and Ralston (2005) suggested that the asymmetry in the flow is due to the strain-induced buoyancy flux, which is stabilizing on ebb tides but

destabilizing on flood tides. In regions of the continental shelf influenced by lateral fresh water inputs, Simpson et al. (1990) independently discovered the same phenomenon and described it as strain-induced periodic stratification (SIPS). In the Liverpool Bay region affected by large horizontal density gradients, Simpson et al. (2002) and Rippeth et al. (2001) found pronounced asymmetry in energy dissipation between the flood and ebb tidal regimes. However, in a recent paper Chant et al. (2007) found that the growth of the tidally driven bottom boundary layer in the Hudson River is primarily driven by the bed stress while the tidal straining only plays a minor role in the entrainment process.

In contrast to the extensive investigations at those estuaries and shelf regions, no observations of tidal variability have been reported in Chesapeake Bay. It is not known if and how the asymmetric tidal mixing will affect the stratification and circulation in the Bay. Tidal ranges inside Chesapeake Bay are generally less than 1 m. In the lower Bay, the tidal current amplitudes vary from 0.5 to 1 ms⁻¹. Over the major portion of the middle reaches

*Corresponding author. Tel.: +1 410 210 8420; fax: +1 410 210 8490.
E-mail address: mingli@hpl.umces.edu (M. Li).

of the Bay, the tidal current is weaker with amplitudes ranging from 0.1 to 0.4 ms⁻¹, but increasing to about 0.6 ms⁻¹ near the head of the estuary (Carter and Pritchard, 1988). Although tides in Chesapeake Bay are weaker than those in the Columbia River and Hudson River, they still play an important role in forcing the Bay (Zhong and Li, 2006). Hence, it is of great interest to find out the variability of mixing and stratification over the flood–ebb tidal cycle.

Over the longer spring–neap tidal cycle, previous observations have revealed significant variations in the tidal current in Chesapeake Bay (e.g. (Browne and Fisher, 1988; Carter and Pritchard, 1988). At springs (neaps) tidal-current amplitudes are about 30–40% higher (lower) than the averaged valued listed above. According to the observations in the Hudson River and elsewhere, such changes in the amplitude of tidal currents would cause dramatic changes in the mixing and vertical stratification in the estuary (Warner et al., 2005a; Peters and Bokhorst, 2000, 2001). In the York and Rappahannock Rivers tributaries of Chesapeake Bay, Haas (1977) and Sharples et al. (1994) indeed found that salinity oscillated between conditions of considerable vertical salinity stratification and homogeneity on a cycle that was closely related with the spring–neap tidal cycle. However, it is not known how the spring–neap tidal cycle affects the stratification and circulation in the main stem of Chesapeake Bay.

One-dimensional models have been used to investigate the flood–ebb asymmetry at single stations in estuaries or shelf regions affected by freshwater discharge. For example, Simpson et al. (2002) used 1D k - ϵ turbulence closure model to explain the observed semi-diurnal cycle of dissipation in a Region of Freshwater Influence in the Irish Sea. Their model produced a realistic description of energy dissipation and its asymmetric behaviour on ebb and flood. Despite these interesting studies in recent years, several key questions on the flood–ebb tidal asymmetry remain unanswered. What are the relative roles of baroclinic pressure gradient and tidal straining in estuarine dynamics? Is the flood–ebb mixing asymmetry caused by the flood–ebb asymmetry in the bed stress (e.g. Geyer et al., 2000) or due to tidal straining of the density field? An important open question is whether or not the asymmetric tidal mixing affects the residual circulation in estuaries and shelf seas. It is still debated if the estuarine circulation is driven by the baroclinic pressure gradient as hypothesized in the classic theory of Pritchard (1956) or is driven by tidal straining and asymmetric tidal mixing as proposed in recent papers (e.g. Jay and Smith, 1990; Stacey et al., 2001).

In this paper we use a realistic three-dimensional (3D) numerical model of Chesapeake Bay to examine the variations of flow and salinity fields over flood–ebb and spring–neap tidal cycles. Our goal is to better understand the relationship between turbulent mixing and estuarine circulation in Chesapeake Bay and gain new insights into the dynamics of estuarine circulation. The Regional Ocean Modeling System (ROMS) is a state-of-art 3D coastal

ocean model (Shchepetkin and McWilliams, 2005). We have configured ROMS for Chesapeake Bay and validated it using time-series of sea level, temperature, salinity and currents from a number of monitoring stations as well as 3D synoptic hydrographic surveys (Li et al., 2005; Zhong and Li, 2006). The model shows considerable capability in reproducing estuarine dynamics at seasonal and annual time-scales. We have also had success simulating extreme events such as hurricanes (Li et al., 2006, 2007). We hope that the modeling results reported in this paper will motivate future observational studies into the tidal variability in Chesapeake Bay.

2. Model description and validation of tidal predictions

We have configured the Regional Ocean Modeling System (ROMS) for Chesapeake Bay. Fig. 1 shows model's bathymetry and its horizontal grid system. The bathymetry is extracted from high-resolution Coastal Relief Model data archived at NOAA's National Geophysical Data Center. We have selected a model domain that includes the main stem of the Bay as well as eight major tributaries. The domain also includes a piece of the coastal ocean so that sea level height at the open boundary can be prescribed using a coarse-resolution global tidal model. We have designed an orthogonal curvilinear coordinate system to follow the general orientation of the deep channel and the coastline of the main stem. The grid size is less than 1 km in the cross-channel direction and 2–3 km in the along-channel direction. The total number of grid points is 120 × 80. The model has 20 layers in the vertical direction. The stretching parameters for the vertical grid are $\theta_S = 2$ and $\theta_B = 0.8$, as defined in the S-coordinate system (Song and Haidvogel, 1994). The ROMS model uses a turbulence closure model to calculate vertical viscosity and diffusivity (Warner et al., 2005b). Li et al. (2005) compared k - kl (modified Mellor–Yamada), k - ϵ , k - ω and KPP closure models and found that they produced similar salinity and diffusivity predictions. In this paper we choose k - ϵ model with the background diffusivity and viscosity set at 10⁻⁵ m² s⁻¹. Coefficients of horizontal eddy viscosity and diffusivity are set to 1 m² s⁻¹. We specify a bottom stress using the drag law

$$\frac{\tau}{\rho} = C_d u |u|_{z=\Delta z/2},$$

where the drag coefficient is calculated from

$$C_d = \frac{u_*^2}{u^2|_{z=\Delta z/2}} = \frac{k^2}{[\log \Delta z/2/z_0]^2}$$

with Δz being the grid size at the lowest grid point, z_0 the roughness height and $k = 0.4$ the von Karman constant. In the model, we specify z_0 according to the reported bottom type used in previous studies (e.g. Xu et al., 2002). A more detailed description of this numerical model can be found in Li et al. (2005).

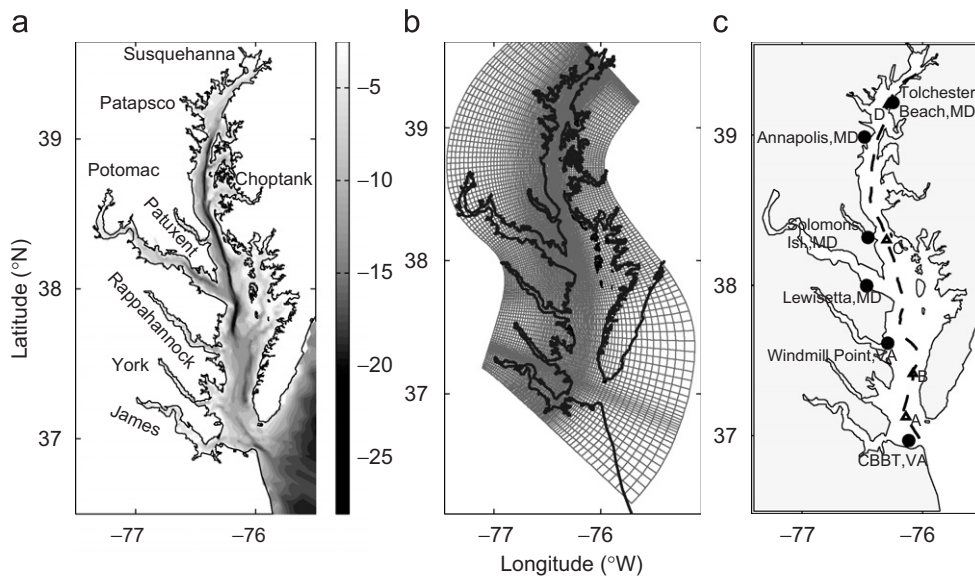


Fig. 1. (a) Bathymetry of Chesapeake Bay and its adjacent coastal area. Major tributaries are marked. Depths are in meters. (b) A horizontal curvilinear coordinate system designed for resolving the complex coastlines and the deep channel in the Bay. (c) Locations for the longitudinal transect (dashed line) used in the model analysis. The filled circles are water-level gauge stations. The triangle symbols represent stations A, B, C and D where time series analysis is conducted.

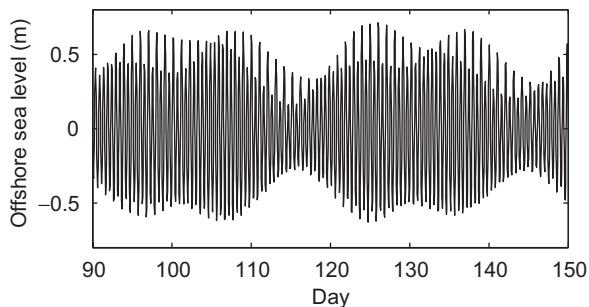


Fig. 2. Time series of the offshore sea level obtained from OSU global tidal model.

Tidal forcing at the open ocean boundary is specified using Oregon State University (OSU) global inverse tidal model of TPXO.6.2, which solves the Laplace tidal equations with a grid resolution of 0.25 by 0.25 and assimilates data from tidal gauge observations and TOPEX/Poseidon satellite measurements (Egbert et al., 1994; Egbert and Erofeeva, 2002). Tidal elevation at the open boundary is decomposed into five major tidal constituents, M_2 , S_2 , N_2 , K_1 , O_1 , using the harmonic constants linearly interpolated from OSU global tidal model. These five constituents account for about 95% of total tidal sea level variability while the interaction among the three semi-diurnal constituents (M_2 , N_2 and S_2) generates fortnightly and monthly variability in the tidal currents (Browne and Fisher, 1988). Fig. 2 shows the time series of sea level at an offshore station. The open-ocean boundary condition consists of a Chapman's condition for surface elevation and a Flather's condition for barotropic velocity. An Orlandi's type radiation condition is used for baroclinic velocity, and a combination of radiation

condition and nudging (with a relaxation time scale of 1 day) are specified for temperature and salinity. Salinity and temperature fields on the offshore open boundary are prescribed using monthly Levitus climatology (Levitus, 1982) combined with field data at Duck, North Carolina, acquired by the Field Research Facility of the US Army Corps of Engineers.

At the upstream boundary in each tributary, daily freshwater inflow with zero salinity is prescribed. On each inflow cross-section, the incoming current is uniform with time-varying speeds regulated by daily freshwater discharge rate. The Chapman radiation condition is used to filter out the outgoing tidal waves at the upstream boundary of each tributary. This paper focuses on the flood-ebb and spring-neap tidal variability so that the freshwater flow rates are kept constant during the model integrations. The total flow rate is fixed at the long-term average of $1500 \text{ m}^3 \text{ s}^{-1}$: 50% is allocated to the Susquehanna River, 20% to the Potomac River, 15% to the James River while the remaining 15% is divided evenly among the five smaller tributaries (Choptank, Patapsco, Patuxent, Rappahannock and York) (cf. Valle-Levinson et al., 1998).

We switched off local wind stress acting on the Bay's surface as well as coastal sea level setup/setdown that could be generated by remote winds blowing along the adjacent shelf. The initial temperature and salinity distributions in the Bay were obtained from one-year model integration using the observed forcing. The model is integrated for a total of 300 days but a quasi-steady state is reached after 60 days.

Since the goal of this paper is to examine the effects of tidal flows on stratification and mixing in Chesapeake Bay, it is important to demonstrate that the model can

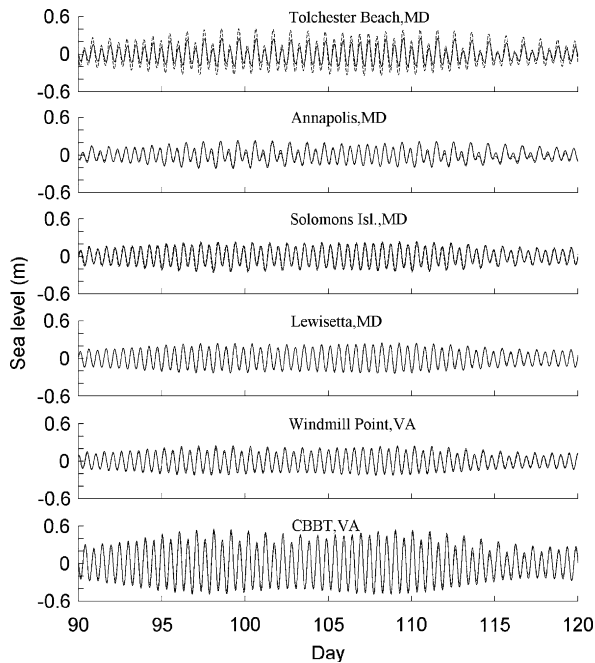


Fig. 3. Time series of observed (solid line) and modeled (dashed line) tidal surface elevations at six tide gauge stations.

accurately predict the tidal heights and tidal currents in the Bay. In Fig. 3 we compare the observed and predicted sea surface elevations at six tidal stations in the Bay. Non-tidal sea level fluctuations were removed using the harmonics method (see Zhong and Li, 2006). Tochester Beach and Annapolis stations are in the upper Bay, Solomons Island and Lewisetta stations in the middle Bay, Windmill Point and CBBT in the lower Bay (see Fig. 1c for their locations). The modeled tidal elevations follow closely the observed records at the lower and middle Bay stations, but the model slightly overpredicts the tidal amplitude at the Tolchester Beach station in the upper Bay. The averaged root-mean-square (rms) error is less than 5 cm, the correlation coefficient greater than 0.95 and the skill score exceeding 0.95. The averaged rms differences between the observed and modeled tidal current ellipses are 2.6, 2.1 cm s^{-1} , 5.11 and 21.71 for the semi-major, semi-minor axes, inclination and phase of the ellipses, respectively (Zhong and Li, 2006). Therefore, the ROMS model accurately predicts both the tidal heights and tidal currents in Chesapeake Bay.

3. Flood–ebb asymmetry

Now we examine how the tidal currents generate turbulent mixing and affect stratification and residual circulation over a flood–ebb cycle. We first conduct a detailed analysis of the flood–ebb cycle at a fixed location and then compare the salinity, diffusivity and subtidal velocity fields in the Bay at different phases of a tidal cycle.

Since previous studies (e.g. Geyer et al., 2000) found that the bottom stress exhibits stronger flood–ebb asymmetry during neap tides than during spring tides, we shall analyse

the flood–ebb asymmetry during both spring and neap tides.

First, we analyse the flood–ebb asymmetry during a spring-tide. Tidal currents are strong in the shallow lower Bay. We select station B (see Fig. 1c for its location) for a detailed analysis of the flood–ebb cycle. As shown in Fig. 4a, the depth-averaged current oscillates at the M_2 frequency. We choose two time slices during the tidal cycle: one representing the peak flood and one representing the peak ebb. In Figs. 4b–d, we compare the vertical profiles of salinity, current and vertical diffusivity between the peak flood and ebb tides. The bottom boundary layer is thicker on flood (about 7 m) than on ebb (about 5 m). The velocity profile shows a subsurface maximum on flood but a nearly linear distribution on ebb. The out-estuary surface slope together with the sloping isopycnals (isohalines) create a non-tidal pressure gradient which changes signs from the seaward direction in a surface layer to the landward direction in a bottom layer. On flood, the non-tidal pressure gradient reinforces the tidal pressure gradient at depth but opposes it near the surface, thus causing the velocity to drop as the water surface is approached. On ebb, the non-tidal pressure gradient works in concert with the tidal pressure in the surface layer but opposes it in the bottom layer. This has resulted in a nearly linear distribution of the mean velocity in the vertical direction.

The ROMS model uses a turbulence closure model to calculate vertical viscosity and diffusivity (Warner et al., 2005b). Turbulent flows are assumed to transport momentum and scalars at the same rate so that the eddy viscosity is identical to eddy diffusivity in the model runs. As shown in Fig. 4d, the maximum vertical diffusivity/viscosity is about twice as large on flood than on ebb. This result is in excellent agreement with that estimated from observations in the Hudson River by Geyer et al. (2000). It is also interesting to note that the strong mixing region penetrates higher on flood, which is a reflection of the thicker bottom boundary layer as shown in Fig. 4b.

To get a complete picture of the flood–ebb asymmetry, we plot the time–depth distributions of current, salinity, and vertical diffusivity and energy dissipation rate over several tidal cycles (Fig. 5). The along-channel current shows alternating flooding and ebbing currents. Most of the flooding currents have a subsurface maximum while the ebbing currents always reach the maximum at the surface (Fig. 5a). Salinity in Chesapeake Bay varies from 0 at its head to about 30 at its mouth. The salinity gradient in the longitudinal direction is about 0.1 psu km^{-1} . Tidal advection across this salinity gradient generates salinity fluctuations at a fixed station. Since the currents vary with depth and are different between the flood and ebb phases, vertical salinity profile shows the periodic variation over a tidal cycle, as shown in Fig. 5b. During the ebb phase, less saline water from upstream is advected to the station, resulting in stronger capping of fresh water in the top few meters. In contrast, during the flood phase, more saline water of oceanic origin is brought to the station, producing a pulse

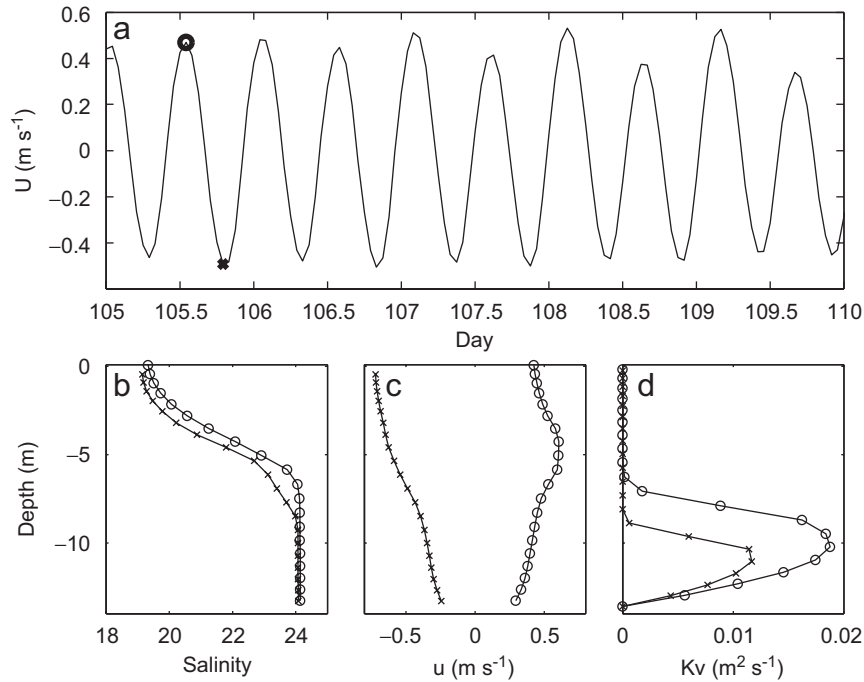


Fig. 4. (a) Time series of along-channel barotropic tidal current velocity at station B. Vertical profiles of (b) salinity, (c) current and (d) eddy diffusivity at the peak flood (open circles) and peak ebb (crosses).

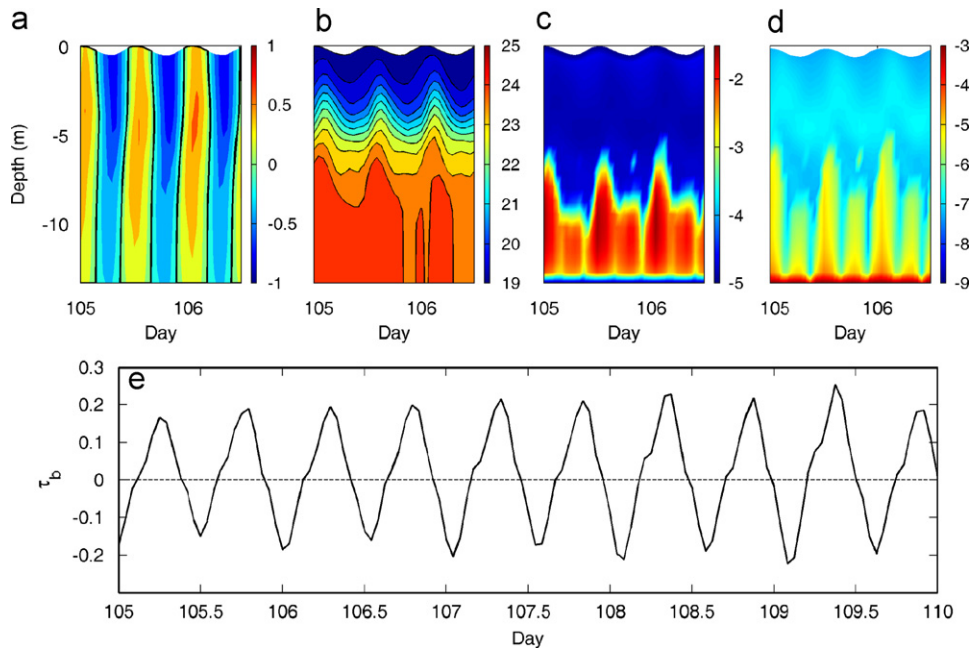


Fig. 5. Time-depth distributions (2.5-day long) of (a) current (m s^{-1}), (b) salinity, (c) logarithm of eddy diffusivity ($\text{m}^2 \text{s}^{-1}$), (d) logarithm of energy dissipation rate (W m^{-3}) and (e) time series (5-day long) of bed stress (N m^{-2}) at station B over the flood–ebb tidal cycles. In (a), zero current speeds are marked by thick black lines. In (b), the hatched area indicates low-salinity surface water.

of higher salinity water in the bottom few meters. This asymmetry in the vertical salinity profile appears to be related to the tidal straining effect (e.g. Simpson et al., 1990), but the small stratification difference observed between the flood and ebb tides suggests that horizontal advection could also play a role.

Now we assess how the tidal currents and salinity stratification affect turbulent mixing and energy dissipation in the water column. Fig. 5c shows a clear asymmetry in the vertical diffusivity over the flood–ebb tidal cycle: strong mixing region penetrates higher on floods than on ebbs. The vertical profiles of energy dissipation rates ε tell a

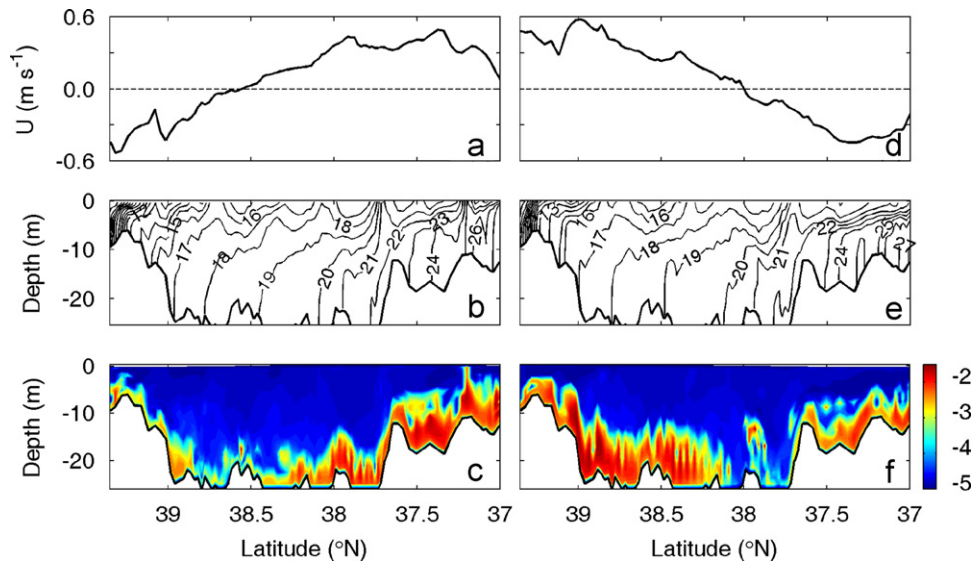


Fig. 6. Along-channel distributions of ((a), (d)) along-channel barotropic tidal current velocity, ((b), (e)) salinity and ((c), (f)) logarithm of vertical diffusivity ($\text{m}^2 \text{s}^{-1}$) at time when the tide is in the flood phase in the lower and middle Bay (day 109.2) or when the tide is in the ebb phase in the lower Bay (day 109.4).

similar story: high ε region extends higher into the water column on flood than on ebb, even though the highest dissipation is confined close to the bottom boundary (Fig. 5d). Therefore, the model results have demonstrated a flood–ebb asymmetry in turbulent mixing. Like other estuaries and shelf seas, Chesapeake Bay is also exposed to this complexity of variable mixing inside a tidal cycle.

In addition to the tidal straining effect discussed above, the bed stress may be stronger on flood than on ebb. For example, Geyer et al. (2000) found significant flood–ebb asymmetry in the bed stress in the Hudson River estuary. This asymmetry in the bed stress could also be a cause for the stronger mixing on the flood tide. During the flood tide, the addition of barotropic tidal pressure gradient and landward-directed baroclinic pressure gradient in the lower layer of the estuary produces stronger current shear near the bottom boundary and hence larger bed stress. During the ebb tide, however, the opposition between the tidal pressure gradient and the baroclinic pressure gradient reduces the current shear near the bottom, thus resulting in smaller bed stress. However, as shown in Fig. 5e, the flood–ebb asymmetry in the bed stress is relatively small during this spring tide period. Later we will check this asymmetry during the neap tide.

So far we have focussed our discussions on a single station in the Bay. Since the magnitude and phase of tidal currents vary in the Bay, it is of interest to examine how the flood–ebb asymmetry affects the Bay as a whole. In Fig. 6, we plot the distributions of salinity and vertical diffusivity in a vertical section aligned with the center axis of Chesapeake Bay (see Fig. 1c for its location). Because the Bay is long, a complete M_2 tidal wave can be placed inside the Bay. To indicate the phase of tide, we plot the barotropic tidal current in the same along-channel section. We compare the along-channel distributions at two

different times of a tidal cycle. Figs. 6a–c correspond to a time (day 109.2, see Fig. 4a) when the tide current is in the flood phase from the Bay mouth to 38.5° latitude but switches to the ebb phase north of this latitude. Turbulent mixing is much stronger south of the dividing latitude where the tide is flooding. Turbulent mixing is weak north of the dividing latitude where the tide is ebbing. In Figs. 6d–f, the tides are in an opposite phase (day 109.4) when the tide is in the ebb phase in the lower and part of the middle bay but in the flood phase in the upper bay. Notice that the dividing latitude between the flooding and ebb flows now shifts to roughly 38° latitude. Interestingly, stronger mixing is now found north of 38° , although strong mixing still occurs in the tidally energetic shallow lower Bay (but significantly weaker than that at day 109.2). If we compare the instantaneous diffusivity distributions (Figs. 6c and f) with the tidally averaged diffusivity distribution (Fig. 7b), we find marked variations over the flood–ebb tidal cycle. Although the averaged diffusivity distribution shows a relatively uniform bottom boundary layer everywhere, the instantaneous distributions reveal a north–south asymmetry that shifts with the phase of the tides. Therefore, the flood–ebb asymmetry in the tidal mixing translates into a periodic switching of the S–N asymmetry of turbulent mixing in the long estuary of Chesapeake Bay.

Changes in the salinity distribution over the flood–ebb tidal cycle can be clearly demonstrated if we look at the departure from the tidally averaged salinity. Fig. 7a shows the tidally averaged salinity distribution in the along-channel section. Figs. 7c and d show the difference between the instantaneous salinity distributions and the averaged distribution at two times. In Fig. 7c (day 109.2), positive salinity anomaly up to 2 is found in the lower bay as the flood tide brings in higher salinity shelf water into the Bay. In contrast, negative salinity anomaly up to 2 appears in

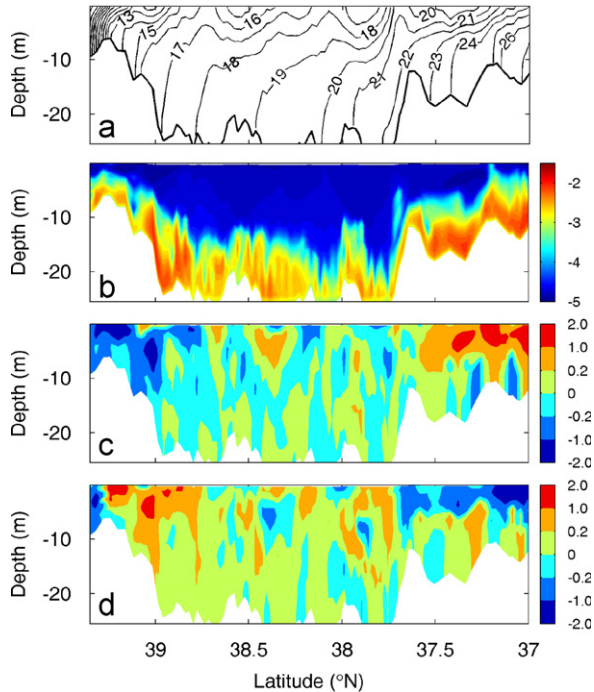


Fig. 7. Along-channel distributions of (a) tidally averaged salinity and (b) logarithm of tidally averaged vertical diffusivity. Difference between the instantaneous and tidally averaged salinity distribution at two times: (c) when the lower Bay is flooding (day 109.2); (d) when the lower Bay is ebbing (day 109.4).

the upper Bay as the fresh river water is carried further downstream by the ebbing tide. Over the mid Bay region (between latitudes 37.6 and 38.7) where the tidal currents are relatively weaker, the salinity anomaly is within 0.2 and of both signs. The salinity anomaly pattern is reversed in sign at the second time (day 109.4), as shown in Fig. 7d. Negative salinity anomaly is now found in the lower bay because the ebb tide exports lower salinity water seaward, but positive salinity anomaly is found in the upper and part of mid bay due to the import of higher salinity by the flood current. Again, relatively small salinity changes are detected in the middle part of the Bay where tidal currents are weak.

We have shown that the turbulent mixing exhibits significant flood–ebb asymmetry while the stratification change is pronounced in the upper and lower Bay but relatively small in the mid-Bay. How does this tidal asymmetry affect the residual circulation and subtidal transport in the estuary? To address this question, we used the harmonics analysis method to remove the tidal-velocity component from the current field. The least-square error method developed by Pawlowicz et al. (2002) was used to calculate harmonic constants for the five major tidal constituents (M_2 , S_2 , N_2 , K_1 , O_1) from two months of current time series at each model grid point. Fig. 8 compares two snapshots of the non-tidal residual velocity with the tidally averaged current in the along-channel section. As one can see, there are only minor changes in the subtidal current within a tidal cycle. Therefore, it appears

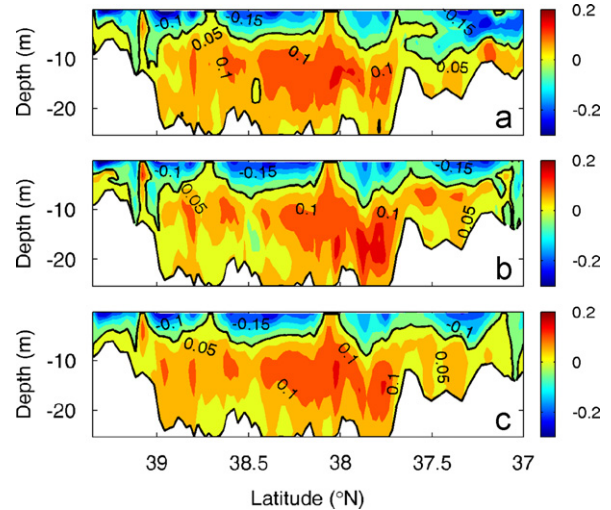


Fig. 8. Along-channel distributions of detided residual current (m s^{-1}) at (a) day 109.2 (a), (b) day 109.4 and (c) tidally averaged current.

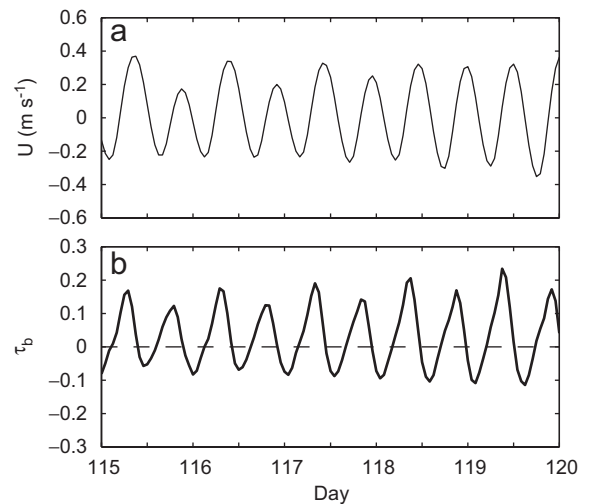


Fig. 9. Time series of (a) depth-averaged current (m s^{-1}) and (b) bed stress (Nm^{-2}) at station B over flood–ebb tidal cycles around the neap tide.

that the flood–ebb mixing asymmetry does not significantly affect the residual gravitational circulation in Chesapeake Bay.

The above results are obtained during the spring tide. Do they apply to the neap tide? To answer this question, we examined a 5-day period during a neap tide. As shown in Fig. 9a, the depth-averaged tidal current is weaker (compare with Fig. 4a). However, the bottom stress exhibits a strong asymmetry between the flood and ebb tides (Fig. 9b). The stress at the peak flood reaches 0.2 Nm^{-2} whereas the stress at peak ebb is about 0.1 Nm^{-2} . Since the neap tide has relatively weak tidal energy, the bottom boundary layer does not get fully developed and the stratification reaches near the seabed. As a result, the bed stress shows stronger flood–ebb asymmetry during the neap tide. This agrees with observations in other estuaries (e.g. Geyer et al., 2000).

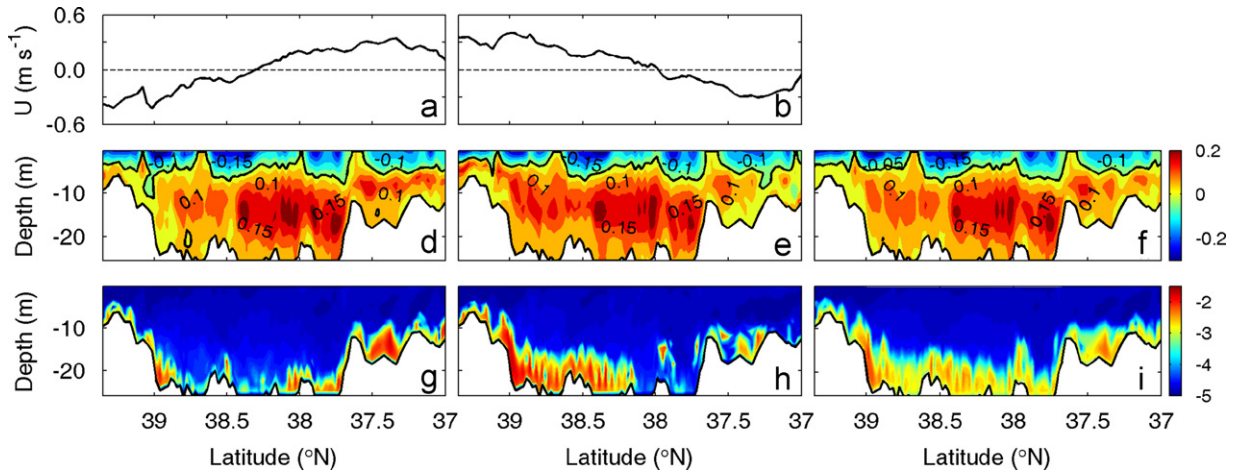


Fig. 10. Along-channel distributions of ((a), (b)) barotropic tidal current speed, ((d), (e)) detided residual current (m s^{-1}) and ((g), (h)) logarithm of vertical diffusivity ($\text{m}^2 \text{s}^{-1}$) at time when the tide is in the flood phase in the lower and middle Bay (day 119) or when the tide is in the ebb phase in the lower Bay (day 119.25). Along-channel distributions of (f) the tidally averaged current and (i) vertical diffusivity ($\text{m}^2 \text{s}^{-1}$).

How does this strong bottom-stress asymmetry affect turbulent mixing and residual circulation in Chesapeake Bay during the neap tide? In Fig. 10, we plot the along-channel distributions of subtidal current and vertical eddy diffusivity at two different phases of a tidal cycle and compare them with the tidally averaged current and diffusivity. The vertical diffusivity in the bottom boundary layer is appreciably larger in regions where the tide is flooding (compare Figs. 10a and g, b and h). However, the subtidal residual current only shows small variations within the tidal cycle and is nearly identical to the tidally averaged current. Therefore, the residual circulation does not appear to be affected by the flood–ebb asymmetry during the neap tides. The same result was found during the spring tides (see Fig. 8). As discussed in the introduction section, a major open question in estuarine dynamics is if the residual circulation is driven by baroclinic pressure gradient or by tidal straining and asymmetric tidal mixing. Our model results which reveal little flood–ebb variability in the subtidal currents suggest that the baroclinic pressure gradient may be the dominant driving force for the residual circulation in a partially mixed estuary such as Chesapeake Bay.

4. Spring–neap cycle

Tidal forcing in Chesapeake Bay is predominantly semi-diurnal (Browne and Fisher, 1988). The interaction among the three semi-diurnal tidal constituents (M_2 , N_2 and S_2) generates fortnightly and monthly variability in the tidal currents. How does this variability affect mixing, stratification and residual circulation in the Bay?

To analyse the spring–neap variability, we selected three stations: station A in the lower Bay, station C in the mid-Bay and station D in the upper Bay (see Fig. 1c for their locations). At the lower-Bay station A, the tidal currents show both fortnightly and monthly cycles (Fig. 11a). The

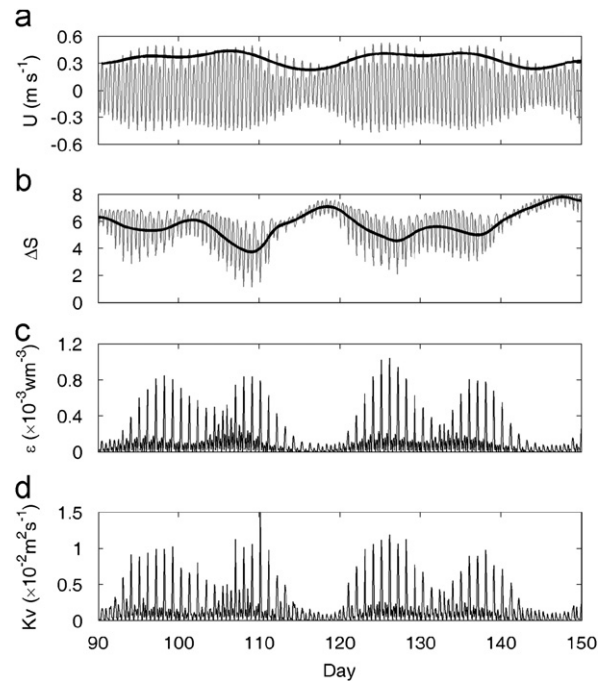


Fig. 11. Time series of (a) barotropic tidal current speed (thin solid), (b) top-to-bottom instantaneous (thin solid) and tidally averaged (thick solid) salinity difference, (c) depth-averaged dissipation rate and (d) eddy diffusivity at station A in the lower Bay. The thick solid line in (a) indicates the tidal-current amplitude.

tidal-current amplitude varies from 0.5 ms^{-1} at the strongest spring to 0.2 ms^{-1} at the weakest neap. In Fig. 11b, we show the salinity difference between the surface and bottom waters. The maximum salinity stratification is about 8 whereas the minimum stratification is nearly 2. In addition to the large spring–neap transition, there are significant flood–ebb fluctuations as discussed earlier. The relationship between the tidal currents and vertical stratification appears to be highly non-linear. Maximum stratification is

reached on days 118 and 147 when the tidal currents are weakest. The two moderate neaps at days 103 and 133 only cause modest rebound in the vertical stratification.

Turbulence kinetic energy production is proportional to the cube of tidal current speed. A small change in the tidal current speed can result in large changes in the turbulent kinetic energy available for mixing. As shown in Fig. 11c, the depth-averaged energy dissipation rate exhibits strong fluctuations over the spring–neap tidal cycles. The peak dissipation rate on springs is 8 times as large as that on the weak neaps. In Fig. 11d, we plot the time series of the depth-averaged vertical diffusivity. The peak diffusivity reaches $0.01 \text{ m}^2 \text{ s}^{-1}$ during the spring tides but is reduced to $0.005 \text{ m}^2 \text{ s}^{-1}$ during the moderate neaps and $0.001 \text{ m}^2 \text{ s}^{-1}$ during the weak neaps. There is an order of magnitude difference in the vertical diffusivity between the neap and spring tides. It is interesting to note that turbulence mixing remains at low levels over several (about 5) days (around days 118 and 147).

In comparison with the strong variability in the lower Bay, the spring–neap signal at a mid-Bay station C is much subdued, as shown in Fig. 12. The top-to-bottom salinity difference shows stronger fluctuations over the flood–ebb cycle than over the spring–neap cycle. The tidally averaged salinity stratification varies within a narrow range of 0.5 around its mean of 3 (Fig. 12b). Because of the weak tidal currents, the vertical diffusivity and energy dissipation rate are much smaller than those at the energetic lower Bay and

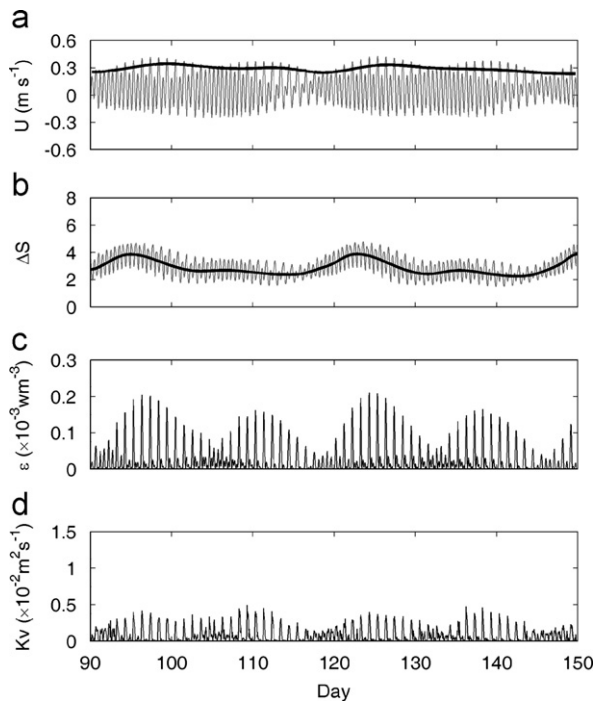


Fig. 12. Time series of (a) barotropic tidal current speed (thin solid), (b) top-to-bottom instantaneous (thin solid) and tidally averaged (thick solid) salinity difference, (c) depth-averaged dissipation rate and (d) eddy diffusivity at station C in the mid-Bay. The thick solid line in (a) indicates the tidal-current amplitude.

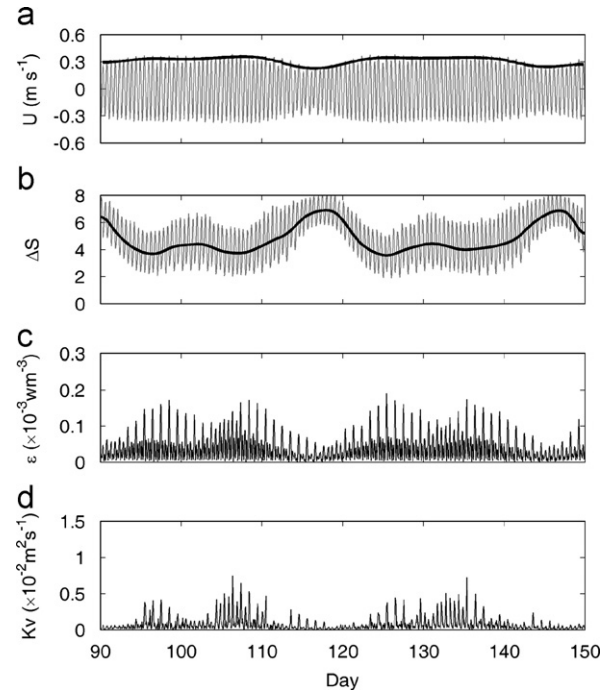


Fig. 13. Time series of (a) barotropic tidal current speed (thin solid), (b) top-to-bottom instantaneous (thin solid) and tidally averaged (thick solid) salinity difference, (c) depth-averaged dissipation rate and (d) eddy diffusivity at station D in the upper Bay. The thick solid line in (a) indicates the tidal-current amplitude.

show relatively small fluctuations over the spring–neap cycle.

At the upper Bay station D, the tidal currents become strong again due to the convergent coastlines and reflections from the estuary head, as shown in Fig. 13a. The tidally averaged surface-to-bottom salinity difference changes from 4 on neaps to 6 on springs (Fig. 13b). The depth-averaged energy dissipation rate and diffusivity exhibit both fortnightly and monthly oscillations (Figs. 13c and 13d). Low mixing that lasts over several days around days 118 and 147 allows significant stratification to build up in the water column. In comparison, no significant rebound in stratification is observed during the neap tides around days 113 and 133. Therefore, in order to build up substantial stratification during the neap tides, weak turbulent mixing needs to persist for a certain length of time.

We have shown that the slow variation of the tidal-current amplitude over the spring–neap cycle causes dramatic changes in mixing and stratification at fixed stations in the Bay. How does this variability affect the Bay as a whole? In Fig. 14 we compare the along-channel distributions of salinity, vertical diffusivity and tidally averaged current between the spring and neap tides. Unlike other estuaries which may transform from a homogeneous to stratified estuary over the spring–neap tide, the salinity distribution in Chesapeake Bay only shows modest changes between the spring and neap tides (Figs. 14a and d). The top-to-bottom salinity difference is about 1 to 2 larger on

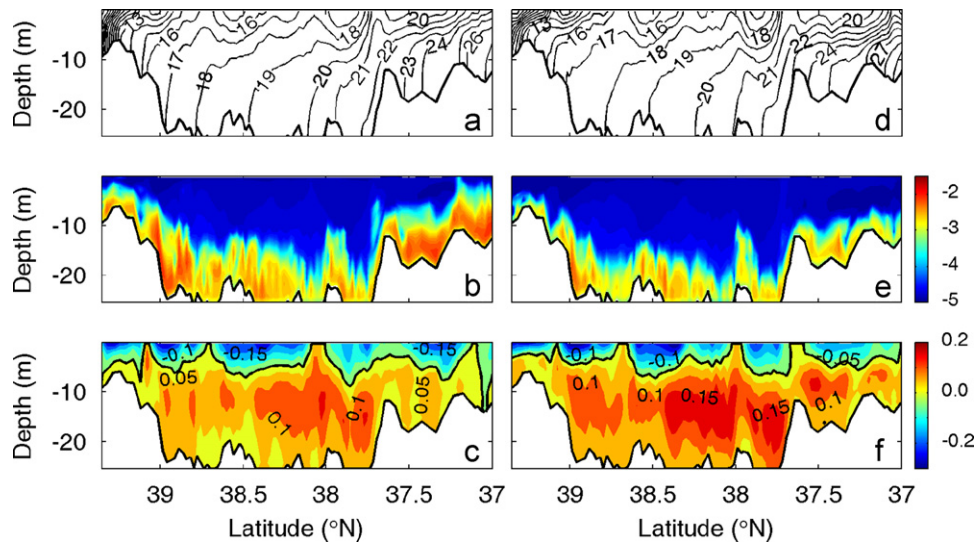


Fig. 14. Along-channel distributions of ((a), (d)) salinity, ((b), (e)) logarithm of vertical diffusivity ($\text{m}^2 \text{s}^{-1}$) and ((c), (f)) tidally averaged residual currents (m s^{-1}) at the spring (day 109) or neap (day 116.5) tides.

the neap than on the spring, which is nevertheless significant compared with the averaged salinity stratification of 2–10 in the Bay. The bottom boundary layer is higher and more energetic on spring (Fig. 14b) than on ebb (Fig. 14e). The averaged diffusivity is $0.0024 \text{ m}^2 \text{ s}^{-1}$ at spring and $0.0014 \text{ m}^2 \text{ s}^{-1}$ at neap so that there is nearly a factor of 2 difference in the strength of vertical mixing between the spring and neap tides.

As shown in Figs. 14c and f, the circulation strength is stronger during the neap tides. The landward return flow increases by 50%. The strength of residual estuarine circulation depends on the competition between the estuary's head-to-mouth density gradient and vertical momentum fluxes. In more turbulent conditions such as during spring tides, more momentum imparted to the circulation by virtue of the horizontal density gradient is diffused vertically, resulting in slower circulation. As shown in Figs. 14b and e, strong mixing/vertical momentum exchange is confined to the upper and lower Bay regions during the spring tide. In contrast, the mixing intensity and stratification in the mid-Bay show relatively moderate changes between the spring and neap tides (compare Figs. 14a and c). Nevertheless, the intense mixing in the southern and northern ends of the Bay creates two choke regions that inhibit horizontal flow exchanges and suppress the gravitational circulation during the spring tide. When turbulence mixing is reduced during the neap tides, these choke regions are removed so that the horizontal density/pressure gradient is able to drive stronger gravitational circulation in the estuary.

5. Conclusion

We have used a numerical model to investigate how flood–ebb and spring–neap tidal cycles affect turbulent mixing, stratification and residual circulation in Chesapeake Bay.

Vertical profiles of salinity, velocity, eddy diffusivity and energy dissipation rates show a marked asymmetry between the flood and ebb tides. This flood–ebb asymmetry results in a north–south asymmetry in turbulent mixing because tidal currents vary out of phase between the lower and upper regions of Chesapeake Bay. The asymmetric tidal mixing causes significant variation of salinity distribution over the flood–ebb tidal cycle. However, there are only minor changes in the subtidal currents within a tidal cycle. Therefore, it appears that the flood–ebb mixing asymmetry does not significantly affect the residual gravitational circulation in Chesapeake Bay.

Previous investigations have convincingly demonstrated that tidal straining causes flood–ebb asymmetry in mixing and stratification in estuaries and shelf seas affected by river runoff. However, it has not been shown how the asymmetric tidal mixing affects the residual circulation. It remains unclear and hotly debated if the estuarine circulation is driven by the baroclinic pressure gradient as hypothesized in the classic theory of Pritchard (1956) or is driven by tidal straining and asymmetric tidal mixing as proposed in recent papers (e.g. Jay and Smith, 1990; Stacey et al., 2001). Our model results which reveal little flood–ebb variability in the subtidal currents suggest that the baroclinic pressure gradient is the dominant driving force for the residual circulation in a partially mixed estuary such as Chesapeake Bay.

Due to the modulation of tidal currents over the spring–neap cycle, turbulent mixing and vertical stratification show large fortnightly and monthly fluctuations in Chesapeake Bay. The stratification appears to be a highly non-linear function of the tidal-current amplitude. Small changes in the tidal currents cause large changes in the eddy diffusivity and energy dissipation rates, but the stratification build-up depends not only on the magnitude of the mixing coefficient but also on its time history. Strong

stratification is only established during those neap tides when low turbulence intensity persists for several days. We also found that the residual circulation shows large variation over the spring–neap cycle. The tidally averaged residual currents are about 50% stronger during the neap tides than during the spring tides. Masson and Cummins (2000) used a numerical model to investigate how the spring–neap cycle affects the estuarine circulation in Juan de Fuca Strait on the west coast of North America. They imposed a fortnightly modulation on the mixing coefficient over the sills connected to the Strait and found that the resulting variation in the estuarine circulation was largely limited to the eastern section of the Strait. This result is not inconsistent with the result reported here since turbulent mixing is confined to the sills in the fjord-estuary of Juan de Fuca Strait but is broadly distributed in the coastal plain estuary of Chesapeake Bay.

Results presented in this paper are based on the outputs from a numerical model. Although this model have been validated against a variety of observational data (e.g. Li et al. 2005, 2006; Zhong and Li, 2006), there are to our knowledge no existing data with adequate temporal resolution to resolve the flood–ebb and spring–neap tidal cycles in Chesapeake Bay. The Chesapeake Bay Program maintains a number of monitoring stations in the Bay but the sampling frequency is biweekly to monthly. Our model results which reveal significant variability in salinity distribution and residual circulation over the spring–neap cycle should motivate future observations of tidal variability in Chesapeake Bay.

Acknowledgments

We thank two referees for their thoughtful comments. This work is supported by grants from NOAA Chesapeake Bay Program (NCBO) and CICEET. This is UMCES contribution number 4106.

References

- Browne, D.R., Fisher, C.W., 1988. Tide and tidal currents in the Chesapeake Bay. NOAA Technical Report NOS OMA 3, 84 pp.
- Carter, H.H., Pritchard, D.W., 1988. Oceanography of Chesapeake Bay. In: Kjerfve, B. (Ed.), *Hydrodynamics of Estuaries: Dynamics of Partially-mixed Estuaries*, vol. 1. CRC Press, pp. 1–16.
- Chant, R.J., Geyer, W.R., Houghton, R., Hunter, E., Lerczak, J., 2007. Estuarine boundary layer mixing processes: insights from dye experiments. *Journal of Physical Oceanography*, in press.
- Egbert, G.D., Bennett, A., Foreman, M., 1994. TOPEX/Poseidon tides estimated using a global inverse model. *Journal of Geophysical Research* 99 (C12), 24,821–24,852.
- Egbert, G.D., Erofeeva, S.Y., 2002. Efficient inverse modeling of barotropic ocean tides. *Journal of Atmospheric and Oceanic Technology* 19 (2), 183–204.
- Geyer, W.R., Trowbridge, J.H., Bowen, M.M., 2000. The dynamics of a partially mixed estuary. *Journal of Physical Oceanography* 30, 2035–2048.
- Haas, L.W., 1977. The effect of the spring-neap tidal cycle on the vertical salinity structure of the James, York and Rappahannock Rivers, Virginia, USA. *Estuarine and Coastal Marine Science* 5, 485–496.
- Jay, D.A., Smith, J.D., 1990. Residual circulation in shallow estuaries. II. Weakly stratified and partially mixed, narrow estuaries. *Journal of Geophysical Research* 95, 733–748.
- Levitus, S., 1982. *Climatological atlas of the world ocean*. NOAA Prof. Pap. 13, US Government Print Office, Washington, DC, 173pp.
- Li, M., Zhong, L., Boicourt, W.C., 2005. Simulations of Chesapeake Bay estuary: sensitivity to turbulence mixing parameterizations and comparison with observations. *Journal of Geophysical Research* 110, C12004.
- Li, M., Zhong, L., Boicourt, W.C., Zhang, S., Zhang, D.-L., 2006. Hurricane-induced storm surges, currents and destratification in a semi-enclosed bay. *Geophysical Research Letters* 33, L02604.
- Li, M., Zhong, L., Boicourt, W.C., Zhang, S., Zhang, D.-L., 2007. Hurricane-induced destratification and restratification in a partially-mixed estuary. *Journal of Marine Research* 65, 169–192.
- Masson, D., Cummins, P.F., 2000. Fortnightly modulation of the estuarine circulation in Juan de Fuca Strait. *Journal of Marine Research* 58, 439–463.
- Pawlowicz, R., Beardsley, B., Lentz, S., 2002. Classical tidal harmonic analysis including error estimates in MATLAB using T_TIDE. *Computers and Geosciences* 28, 929–937.
- Peters, H., Bokhorst, R., 2000. Microstructure observations of turbulent mixing in a partially mixed estuary. Part I. Dissipation rate. *Journal of Physical Oceanography* 30, 1232–1244.
- Peters, H., Bokhorst, R., 2001. Microstructure observations of turbulent mixing in a partially mixed estuary. Part II. Salt flux and stress. *Journal of Physical Oceanography* 31, 1105–1119.
- Pritchard, D.W., 1956. The dynamic structure of a coastal plain estuary. *Journal of Marine Research* 15, 33–42.
- Rippeth, T.P., Fisher, N.R., Simpson, J.H., 2001. The cycle of turbulent dissipation in the presence of tidal straining. *Journal of Physical Oceanography* 31, 2458–2471.
- Sharples, J., Simpson, J.H., Brubaker, J.M., 1994. Observations and modelling of periodic stratification in the upper York River estuary, Virginia. *Estuarine, Coastal and Shelf Science* 38, 301–312.
- Shchepetkin, A.F., McWilliams, J.C., 2005. The regional oceanic modeling system: a split-explicit, free-surface, topography-following-coordinate ocean model. *Ocean Modelling* 9, 347–404.
- Simpson, J.H., Brown, J., Matthews, J., Allen, G., 1990. Tidal straining, density currents, and stirring in the control of estuarine stratification. *Estuaries* 13, 125–132.
- Simpson, J.H., Burchard, H., Fisher, N.R., Rippeth, T.P., 2002. The semi-diurnal cycle of dissipation in a ROFI: model-measurement comparisons. *Continental Shelf Research* 22, 1615–1628.
- Song, Y.T., Haidvogel, D.B., 1994. A semi-implicit ocean circulation model using a generalized topography-following coordinate. *Journal of Computational Physics* 115, 228–244.
- Stacey, M.T., Ralston, D.K., 2005. The scaling and structure of the estuarine bottom boundary layer. *Journal of Physical Oceanography* 35, 55–71.
- Stacey, M.T., Burau, J.R., Monismith, S.G., 2001. Creation of residual flows in a partially stratified estuary. *Journal of Geophysical Research* 106, 17013–17043.
- Valle-Levinson, A., Li, C., Royer, T.C., Atkinson, L.P., 1998. Flow patterns at the Chesapeake Bay entrance. *Continental Shelf Research* 18, 1157–1177.
- Warner, J.C., Geyer, W.R., Lerczak, J.A., 2005a. Numerical modeling of an estuary: a comprehensive skill assessment. *Journal of Geophysical Research* 110, C05001.
- Warner, J.C., Sherwood, C.R., Arango, H.G., Butman, B., Signell, R.P., 2005b. Performance of four turbulence closure models implemented using a generic length scale method. *Ocean Modeling* 8, 81–113.
- Xu, J., Chao, S.-Y., Hood, R. R., Wang, H., Boicourt, W. C., 2002. Assimilating high-resolution salinity data into a model of a partially mixed estuary. *Journal of Geophysical Research* 107, No. C7, pp. 11-1–11-14.
- Zhong, L., Li, M., 2006. Tidal energy fluxes and dissipation in the Chesapeake Bay. *Continental Shelf Research* 26, 752–770.